Analyst

Accepted Manuscript

This article can be cited before page numbers have been issued, to do this please use: C. Zhang, K. Wen, X. Yang and Y. Zhu, *Analyst*, 2019, DOI: 10.1039/C9AN00427K.

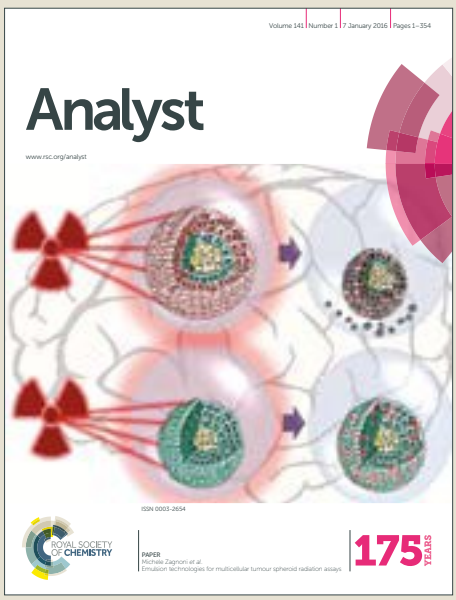

ROYAL SOCIETY OF CHEMISTRY

rsc.li/analyst

View Article Online
DOI: 10.1039/C9AN00427K

ARTICLE

Rolling circle amplification-mediated in-situ synthesis of palladium nanoparticles for ultrasensitive electrochemical detection of microRNA†

Received 00th January 20xx,
Accepted 00th January 20xx

DOI: 10.1039/x0xx00000x

Cuiling Zhang, Kai Wen, Xingdong Yang and Ye Zhu*

An ultrasensitive and label-free electrochemical biosensor for microRNA (miRNA) was developed based on rolling circle amplification (RCA)-mediated palladium nanoparticles (PdNPs). The sensor was fabricated by immobilization of dual functionalized hairpin probes onto the electrode. The specific recognition of target miRNA-21 by the hairpin probes could trigger the RCA reaction which produced numerous guanine (G)-rich long single-stranded DNAs (ssDNAs). Based on the interaction of Pd^{II} species with the nitrogen atoms from G bases, these G-rich long ssDNAs served as specific templates to in-situ synthesize massive PdNPs as electrochemical indicators. The formation of PdNPs was demonstrated by high-resolution transmission electron microscopy to be exactly along the RCA products. With this cascade signal amplification strategy, the developed biosensor achieved a linear range from 50 aM to 100 fM with an ultralow detection limit of 8.6 aM miRNA-21. Furthermore, the developed biosensor exhibited good selectivity, reproducibility, stability and satisfactory feasibility of miRNA-21 detection in human serum samples, ensuring it great potential in disease diagnosis and prognosis applications.

Introduction

MicroRNAs (miRNAs), as promising biomarkers for non-invasive early diagnosis and prognosis of diseases especially cancers, provide essential and pivotal information for understanding cancer initiation, metastasis and further biomedical applications.[1] Analysis of miRNA is of significant meaning. However, the accurate detection of miRNA is still challenging because of their intrinsic properties including small size, low expression levels in biological samples and sequence similarity among family members.[2,3] It is imperative to develop highly sensitive and selective methods to meet the demands for miRNA analysis. Biosensors based on specific molecular recognition are efficient tools for miRNA analysis. In particular, electrochemical biosensors, relying on their inherent advantages of miniaturization, low cost, fast response and convenient operation,[4,5] hold great potential in the development of miRNA analysis-based point-of-care diagnostic devices.

Recently, DNA templated-metal nanoparticles, a class of newly emerged signal reporters, have been revealing promising potential in electrochemical biosensors due to their ease of synthesis, low toxicity, good biocompatibility, good electrochemical properties, as well as sequence dependence.[6-8] For instance, cytosine (C)-rich loop DNA-stabilized silver nanoclusters (AgNCs)[9] and double-stranded DNA-templated copper nanoclusters[10] were employed as electrochemical signal indicators for ultrasensitive and label-free detection of miRNAs. Based on poly(thymine)-templated copper nanoparticles (CuNPs), our group designed a cascade signal amplification strategy for ultrasensitive detection of cancer markers.[11] In addition to DNA-templated AgNCs and CuNPs, DNA-templated palladium nanoparticles (PdNPs) were also investigated and were demonstrated with excellent physical and chemical properties. Highly conductive Pd nanowires synthesized on lambda DNA have been reported.[12,13] Further, Zhang's group discovered that guanine (G)-rich oligonucleotide was suitable template for easily modulating the morphology of PdNPs. Based on the interaction of Pd^{II} ions with the nitrogen atoms from G bases, they synthesized PdNPs with highly catalytic activities in Suzuki coupling reactions.[14] As a class of nanomaterials with superior electroactive and catalytic properties, DNA-templated PdNPs are promising candidates for signal amplification and reporting. However, their potential in bioanalytical applications has been rarely investigated. Considering that the productivity of PdNPs is highly dependent on the length and sequence composition of oligonucleotides,[15] the combination of DNA-templated PdNPs with programmable DNA amplification would be a perfect signal amplification strategy for ultrasensitive bioanalysis.

Rolling circle amplification (RCA) has been introduced into bioanalysis because of its high speed, mild reaction conditions, powerful amplification efficiency and capability of integrating target recognition with signal amplification.[16] In a linear RCA reaction, a short primer can be extended to a long single-

School of Chemistry and Chemical Engineering, Shandong University, Jinan 250100, China. E-mail: zhuye@sdu.edu.cn

† Electronic Supplementary Information (ESI) available: Table S1, Fig.S1, Fig. S2, Fig. S3 and Fig. S4. See DOI: 10.1039/x0xx00000x

View Article Online DOI: 10.1039/C9AN00427H

stranded DNA (ssDNA) with numerous of tandem repeats which are complementary to circular template.[17] Due to the difficulty to obtain direct electrochemical signals of DNA bases, effective signal readout methods to transduce these repeated DNA sequences into detectable electrical signals are vital for biosensors. The most common way to read out the RCA products is hybridization with complementary oligonucleotides which are tethered with various indicators including nanoparticles,[18] ferrocene[19] and enzymes.[20] Compared with this hybridization method involving redundant and time-consuming labelling process, another signal-generating method utilizing DNA-intercalating molecules, such as methylene blue[21] and hemin[22] exhibits considerable convenience and has been widely used to read out RCA products. Inspired by the idea that RCA products can be modulated through the special design of the circular template sequence, programmable RCA products would be perfect signal amplification carrier for DNA-templated PdNPs.

Herein, we designed a label-free electrochemical biosensor based on target-induced RCA reaction and DNA-templated PdNPs for accurate detection of miRNA-21 which is associated with various cancers.[23] In this design, RCA reaction was induced by target miRNA to produce massive G-rich long ssDNAs, which were used as effective templates to in-situ synthesize PdNPs as amplified signal indicators. The amount of these electrochemically active PdNPs was positively related to the level of target miRNA, thus leading to extremely sensitive detection of miRNA-21. The feasibility of the design was verified with gel electrophoresis and electrochemical test. RCA product-mediated PdNPs were characterized by high-resolution transmission electron microscopy and UV-Vis absorption spectra. The experimental conditions that might affect the sensor performance were optimized. The calibration curve and the detection limit for miRNA-21 were determined. Finally, the practical applicability of the developed biosensor for real samples analysis was investigated.

Experimental

Chemical and materials

HPLC-purified DNA and miRNA (listed in Table S1) were obtained from Sangon Biotech Co., Ltd (Shanghai, China). Phi 29 DNA polymerase, T4 DNA ligase, diethyl pyrocarbonate (DEPC), 4-(2-hydroxyethyl)piperazine-1-ethanesulfonic acid sodium salt (HEPES), tris hydrochloride (Tris-HCl), ethylenediaminetetraacetic acid (EDTA) and the solution of deoxyribonucleoside triphosphate (dNTPs) mixture were also obtained from Sangon. Sodium borohydride ($NaBH_4$), potassium ferricyanide ($K_3Fe(CN)_6$) and potassium ferrocyanide($K_4Fe(CN)_6$) were bought from Sinopharm Chemical Reagent Co., Ltd (Shanghai, China). Sodium tetrachloropalladate (Na_2PdCl_4), 6-mercapto-1-heanol (MCH) and tris(2-carboxyethyl)phosphine hydrochloride (TCEP) were purchased from Aladdin (Shanghai, China). TE buffer (10 mM Tris-HCl, 100 mM NaCl, 1.0 mM EDTA, pH 8.0) was used to dilute DNA oligonucleotides. Tris buffer (40 mM Tris-HCl, 10 mM $MgCl_2$, pH 7.8) was used for circular template dissolution. Other reagents were of analytical grade and were used without further purification. Consumables were treated with 0.1% DEPC and sterilized with high-pressure steam. Ultrapure water used in all solutions was obtained with an Ulupure water purification system (resistivity = 18.25 MΩ•cm).

Apparatus

Electrochemical measurements were performed on a CHI760E electrochemistry workstation (Shanghai Chenhua, China) with a conventional three-electrode system including a modified gold working electrode (AuE, Φ = 3 mm), a Ag/AgCl (in saturated KCl) reference electrode and a platinum wire counter electrode. The formation of PdNPs was observed by high-resolution transmission electron microscopy (HRTEM, JEM-2200FS, JEOL, Japan) and UV-Vis spectrophotometer (Hitachi U-290 spectrometer, Japan). Native polyacrylamide gel electrophoresis (PAGE) was performed with a DYCZ-24F electrophoretic device (Beijing Liuyi, China). The PAGE gel was imaged on a Bio-Rad Gel Doc XR+ System (Bio-Rad, Hercules, CA, USA). Agarose gel electrophoresis was performed by using a DYCP-31DN electrophoresis apparatus (Beijing Liuyi, China). The agarose gel was imaged by a Tanon-2500R gel imaging system (Shanghai, China).

Fabrication of the sensor

Before modification, the AuE was polished with alumina slurry (50 nm) and then rinsed with ultrapure water, ethanol and ultrapure water successively to remove the alumina powder and other impurities. The well-polished electrode was electrochemically cleaned in 0.5 M H_2SO_4 with potential sweeping between -0.2 V and 1.6 V until a stable cyclic voltammogram (CV) was obtained. Then, the AuE was washed with ultrapure water and dried with nitrogen. Immediately, the pretreated electrode was incubated with 0.1 μM hairpin probe (HP) for 12 h at 4 ℃. To optimize the orientation of the HP and reduce nonspecific adsorption, the working electrode was blocked with 1 mM MCH for 1 h, then the fabrication of the HP/AuE sensor was completed.

Recognition of miRNA-21 and RCA reaction

Briefly, 5 μL of miRNA-21 with different concentrations was dropped onto the fabricated HP/AuE sensor and incubated for 1 h at 37 ℃, followed by washing to remove the unbound miRNA-21. For subsequent RCA reaction, 10 μL of solution containing 0.25 μM circular template (CT), 0.2 U T4 ligase and 1× T4 ligase buffer was added onto the miRNA-21-hybridized sensor and incubated for 1 h at 37 ℃. Afterwards, the RCA reaction was implemented by the addition of 1 mM dNTPs and 0.2 U phi29 DNA polymerase in 10 μL of RCA buffer and incubated for 1 h at 37 ℃. The resulted RCA products were used as templates for PdNPs synthesis.

Synthesis of PdNPs and electrochemical measurements

View Article Online
DOI: 10.1039/C9AN00427K

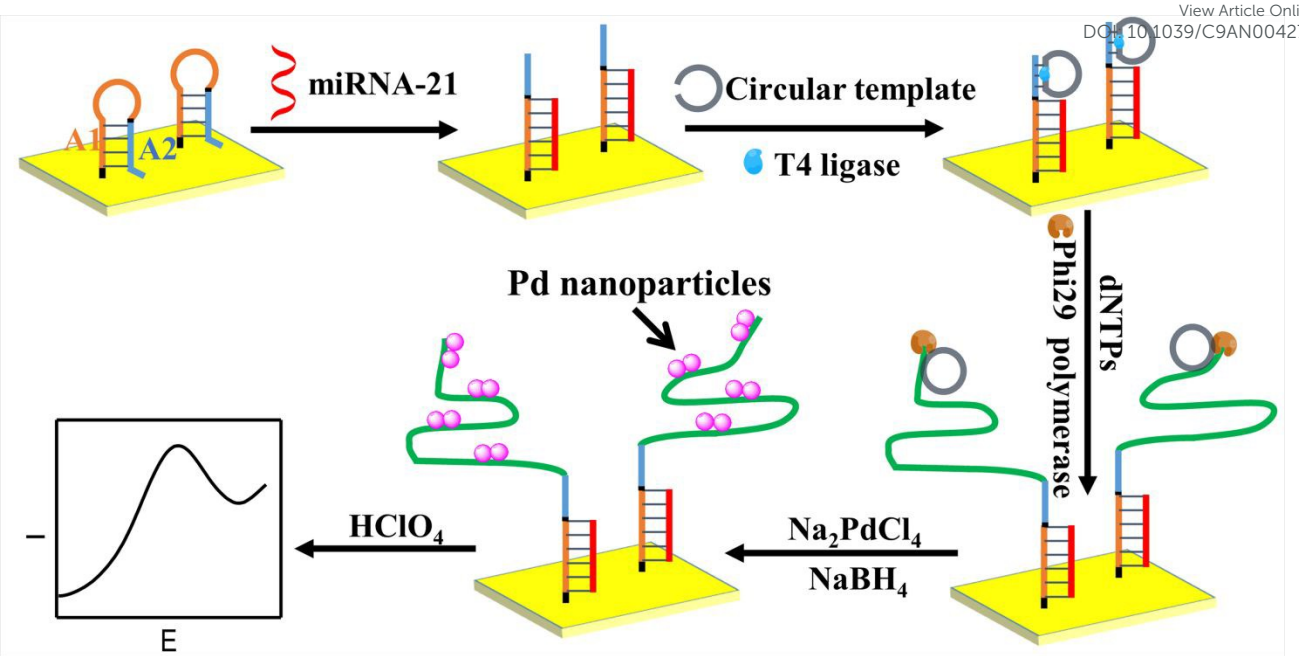

Scheme 1 Schematic illustration of the electrochemical detection of miRNA-21 based on RCA product-mediated synthesis of PdNPs.

After recognition of miRNA-21 and RCA reaction, synthesis of PdNPs was conducted by immersing the resulted electrode into 10 mM HEPES (150 mM KCl, pH 7.5) containing 150 μM Na_2PdCl_4 for 30 min, followed by reduction with 300 μM $NaBH_4$ for 30 min. The reaction proceeded at room temperature and under ambient conditions. To measure the electrochemical signal, differential pulse voltammetry (DPV) was performed in 0.1 M $HClO_4$ from 0.8 V to 1.3 V with an amplitude of 50 mV, a pulse width of 50 ms and a pulse period of 0.5 s.

Gel electrophoresis analysis

Before modification, PAGE was employed to demonstrate the target-induced hybridization of HP and CT. The PAGE was performed in 1× TBE buffer (90 mM Tris, 90 mM boric acid, 2 mM EDTA, pH 8.3) with a constant current of 30 mA for about 1.5 h at 10 ℃. The obtained gel was stained with SYBR gold for 40 min and imaged on the Bio-Rad Gel Doc XR+ System.

Target-induced RCA reaction was verified by agarose gel electrophoresis. Samples were loaded on 0.7% agarose gel, and then electrophoresis was carried out in 1× TAE buffer (40 mM Tris, 20 mM acetic acid, 2 mM EDTA, pH 8.3) at an applied voltage of 120 V for about 1 h at room temperature. After ethidium bromide staining for 15 min, the gel was recorded by using the Tanon-2500R gel imaging system.

Results and discussion

Mechanism of the biosensor

The mechanism of the biosensor is schematically illustrated in Scheme 1. The HP mainly contains two regions: (i) A1 is complementary to miRNA-21; (ii) A2 is a primer of RCA reaction. First, the HPs are self-assembled onto the AuE surface through the formation of Au-S bond. In the presence of miRNA-21, the stem-loop structure of HP is unfolded because of hybridization with miRNA-21, resulting in complete exposure of the A2 region. When T4 ligase and CT are introduced, the exposed A2 region of the HP could hybridize with the CT and further initiate the RCA reaction in the presence of phi29 DNA polymerase and dNTPs. As a result, massive G-rich long ssDNAs are produced by the RCA reaction, which can be used as effective templates for in-situ synthesis of PdNPs and further electrochemical signal transformation. In contrast, in the absence of miRNA-21, HP could keep the stem-loop structure, where half of A2 region hide in the stem. Since the melting temperature between CT and 3′ tail of HP is less

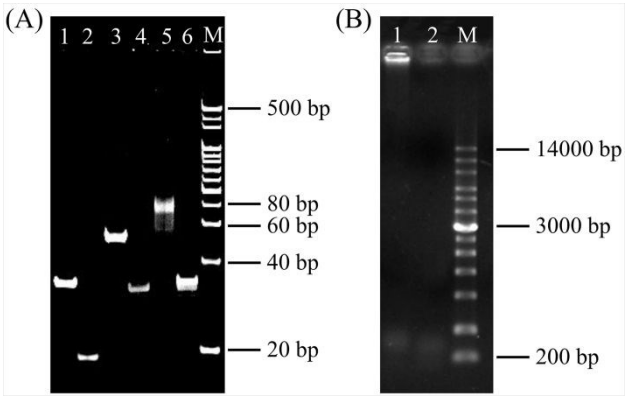

Fig. 1 (A) PAGE images of different samples: (1) HP, (2) miRNA-21, (3) HP + miRNA-21, (4) CT, (5) HP + miRNA-21 + CT + T4 ligase, (6) HP + CT + T4 ligase and (M) marker. (B) Agarose gel electrophoresis analysis: (1) target-induced RCA, (2) control experiment without miRNA-21 and (M) DNA marker.

View Article Online
DOI: 10.1039/C9AN00427K

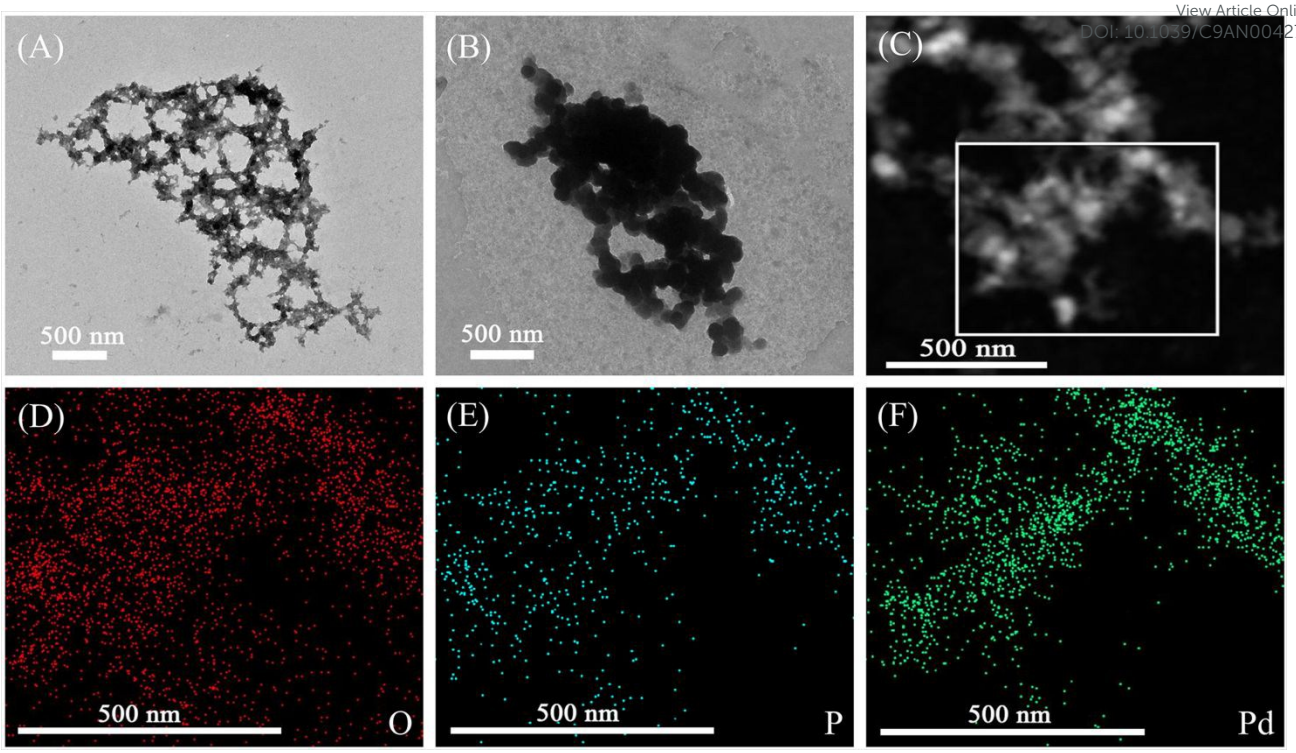

Fig. 2 HRTEM images of (A) RCA product and (B) RCA product-mediated PdNPs. EDS phase distribution images of (C) RCA product-mediated PdNPs for the analysis of (D) O, (E) P and (F) Pd elements.

than 15 ℃, RCA and the following reactions could not be triggered.[24] Thus, the sensitive and selective detection of miRNA-21 could be achieved based on this RCA-mediated PdNPs amplification strategy.

Gel electrophoresis characterization of the design

The PAGE assay was employed to verify the principle of the method. As shown in Fig. 1A, lane 1, 2 and 4 exhibited the band corresponding to HP, miRNA-21 and CT, respectively; while lane 3 exhibited a band with a bp value approximating to the sum of the bands in lane 1 and 2, indicating the successful recognition of miRNA-21 by HP. When the CT and T4 ligase were added, a band with lower mobility than lane 3 appeared (lane 5), suggesting the successful hybridization of CT with the completely exposed A2 region of the unfolded HP. As a control, the HP was directly mixed with the CT and T4 ligase in the absence of miRNA-21. Consequently, the combination of the bands in lane 1 and lane 4 was observed in lane 6, demonstrating that the HP could not hybridize with the CT without the induction of miRNA-21.

The feasibility of target-induced RCA reaction was confirmed by agarose gel electrophoresis (Fig. 1B). RCA reaction based on our design was operated in the presence of miRNA-21, and the obtained product was subjected into lane 1. As a result, a bright band with extremely low mobility appeared in lane 1. According to the indication of DNA marker (lane M), the bases contained in the product was much higher than 14 kbp, suggesting the successful implementation of the target-induced RCA reaction. In contrast, no band was observed in the absence of miRNA-21 (lane 2), suggesting the RCA reaction could not be triggered without miRNA-21. These results were consistent with those obtained by PAGE, demonstrating that the RCA reaction could only occur in the presence of target miRNA-21.

Characterization of RCA product-mediated PdNPs

HRTEM was employed to investigate the formation of PdNPs which were synthesized on RCA product. As shown in Fig. 2, a coil with a diameter of about 2.5 μm was observed for RCA product (image A). This coil might be the buffer salts concentrated around the unextended and coiled DNA strands, which greatly enhanced the image contrast of the RCA product at high electron irradiation.[25,26] After incubating the RCA product with Na_2PdCl_4 and $NaBH_4$, nanoparticles with a diameter around 100 nm were observed (image B), which were clumped together along the similar pattern in image A. To further characterize these particles, element analysis was performed with energy dispersive spectroscopy (EDS) in the selected region of image C. The elemental mapping proved the coexistence of O, P and Pd elements (image D-F). O and P elements were derived from the RCA product, especially P element came from the phosphate backbones of the RCA product. Obviously, the existence of Pd element confirmed the nature of these nanoparticles. More importantly, the distribution of O, P and Pd was basically coincident, suggesting

View Article Online
DOI: 10.1039/C9AN00427K

that the PdNPs were formed only along the RCA product.

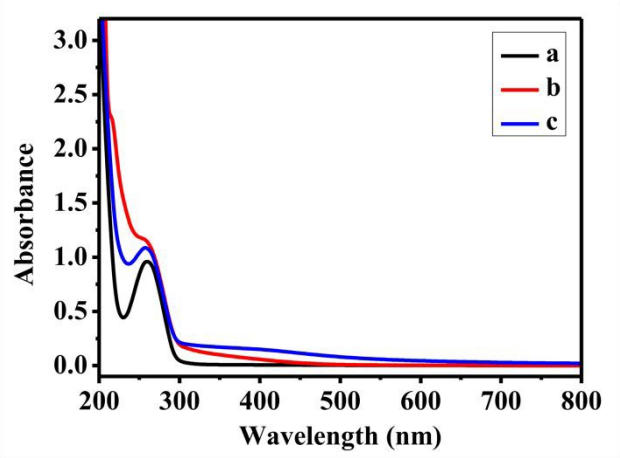

Fig. 3 UV-Vis spectra for (a) G-rich long ssDNA, (b) Na_2PdCl_4/G-rich long ssDNA and (c) PdNPs/G-rich long ssDNA.

These characterizations demonstrated the successful formation of PdNPs using RCA product as an efficient template.

UV-Vis absorption spectra were employed to verify the formation of PdNPs on the RCA produced G-rich long ssDNA. As shown in Fig. 3, the aqueous solution of G-rich long ssDNA exhibited the specific nucleic acid absorption band at 260 nm (curve a). With the addition of Na_2PdCl_4, a ligand-to-metal charge-transfer (LMCT) band was observed around 215 nm in curve b, which was consistent with the interaction of Pd^{II} ions with nitrogen atoms from G bases.[14] After the addition of $NaBH_4$ reductant, the LMCT band disappeared with the appearance of a broad continuous spectrum in the range 300-600 nm (curve c) because of the formation of PdNPs.[14,27,28]

Electrochemical characterization of the biosensor

To confirm the fabrication process of the biosensor and sensing process, electrochemical impedance spectroscopy (EIS) measurements in 0.1 M KCl containing 5.0 mM $[Fe(CN)_6]^{3-/4-}$ were performed to characterize differently modified AuE (Fig. 4A). The inset showed the applied equivalent circuit based on Zview software, which was composed of solution resistance (Rs), constant phase element (CPE), Warburg (diffusion) impedance (Zw) and electron-transfer resistance (Ret). There was a small semicircular domain for bare AuE (curve a), suggesting the fast charge transfer on the bare AuE surface. After incubation with HP and blocking with MCH, an obviously increased Ret with a value of 537.5 Ω was obtained owing to the electrostatic repulsion between the negatively charged phosphate backbones of HP and $[Fe(CN)_6]^{3-/4-}$ anions (curve b),[29] indicating the successful immobilization of HP on AuE. When the fabricated HP/AuE sensor was incubated with miRNA-21, the Ret significantly increased to 1398 Ω (curve c), suggesting that miRNA-21 was recognized and hybridized by the HP immobilized on the sensor. Then, the miRNA-21-hybridized sensor was employed in target-induced RCA

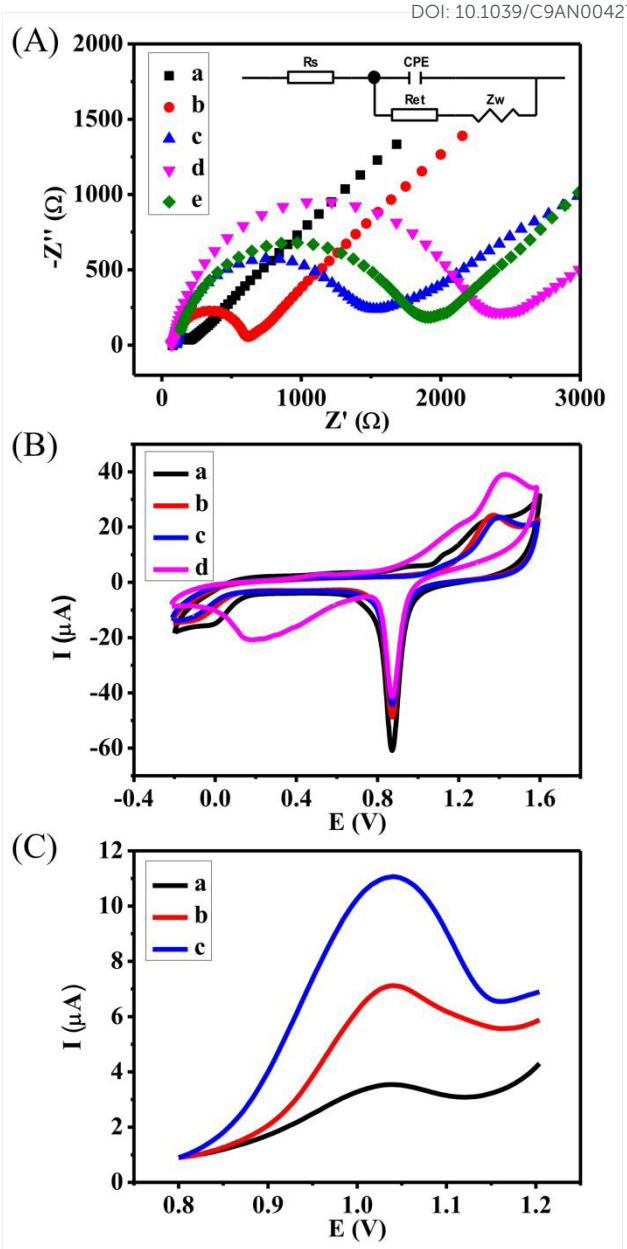

Fig. 4 (A) EIS for (a) bare AuE, (b) HP/AuE, (c) miRNA-21/HP/AuE, (d) RCA product/miRNA-21/HP/AuE and (e) PdNPs/RCA product/miRNA-21/HP/AuE in 0.1 M KCl containing 5.0 mM $[Fe(CN)_6]^{3-/4-}$ in the frequency ranging from 10 mHz to 100 kHz with an amplitude of 5 mV (The inset is the equivalent circuit of the Nyquist plots). (B) CVs for (a) bare AuE, (b) HP/AuE, (c) RCA product/miRNA-21/HP/AuE and (d) PdNPs/RCA product/miRNA-21/HP/AuE in 0.1 M $HClO_4$ by scanning the potential from -0.2 to 1.6 V with a scan rate of 50 mV/s. (C) DPVs of the biosensor in different concentrations of miRNA-21: (a) 0 fM, (b) 1 fM and (c) 100 fM.

reaction and the obtained Ret was further dramatically increased to 2197 Ω (curve d), demonstrating the successful occurrence of the RCA reaction where numerous long ssDNAs were produced and greatly impeded the diffusion of $[Fe(CN)_6]^{3-/4-}$ toward the AuE surface. After the synthesis of PdNPs using the RCA products as templates, the Ret value decreased to 1520 Ω (curve e). That was owing to the

View Article Online
DOI: 10.1039/C9AN00427K

synthesized PdNPs which possessed excellent electronic conductivity and facilitated the electron transfer on the RCA products.

The electrochemical behavior of the designed sensor in 0.1 M $HClO_4$ was studied with cyclic voltammetry in the potential range of -0.2 V - 1.6 V. As shown in Fig. 4B, the bare AuE exhibited a cathodic peak at 0.87 V and anodic peaks between 1.1 V and 1.4 V which were corresponding to gold (curve a). When the AuE was modified with HP and MCH, the cathodic peak clearly decreased and the anodic peaks changed into a single broad anodic peak around 1.4 V because of the coverage of the electrode surface by HP and MCH (curve b). After recognition of miRNA-21 and the following RCA reaction, the resulting sensor showed decreased peak currents due to the coverage of RCA products on the electrode surface (curve c). Further, synthesis of PdNPs on the RCA products was conducted. It was noteworthy that an anodic peak appeared around 1.04 V and a broad cathodic peak rose from 0.8 V in the reverse scan (curve d). According to literature,[30] these two broad peaks were associated with Pd, robustly demonstrating the successful formation of PdNPs. Additionally, the gold-specific cathodic peak at 0.87 V further decreased owing to the coverage of PdNPs on the AuE surface. In particular, it was interesting to observe a distinct anodic peak around 1.45 V. We inferred this peak derived from the oxidation of G base of RCA products which became manifest because of the electrocatalysis of the newly formed PdNPs.[31] These results further demonstrated the successful occurrence of RCA reaction and the resulting formation of PdNPs. Furthermore, the oxidation peak of Pd around 1.04 V was selected and investigated with DPV for miRNA-21 analysis. As displayed in Fig. 4C, there was a small background in the absence of miRNA-21 (curve a), which might be attributed to the coordination of Pd^{II} species with N atoms on nucleobases of the self-assembled HP.[32] In the presence of 1 fM miRNA-21, a significant increase of the peak current was observed due to the formation of massive PdNPs on RCA products (curve b). Moreover, the current response further increased when the concentration of miRNA-21 increased to 100 fM (curve c) because more PdNPs were synthesized on more target-induced RCA products. These results proved the feasibility of the proposed biosensor for miRNA-21 analysis.

Optimization of the experimental conditions

To achieve the best analytical performance of the biosensor, the effect of experimental parameters were investigated, including the concentration of HP, the concentration of CT and the RCA incubation time. Fig. S1A displayed the effect of the HP concentration on the DPV response difference (ΔI) between the presence and absence of miRNA-21. Obviously, ΔI increased with the increasing immobilization concentration of HP and reached the highest value at 0.1 μM HP. In the low concentration range of HP, higher self-assembly density of HP on the electrode surface resulted in more HP-miRNA-21 binding events accompanying higher signal output. However, when the self-assembly density of HP was too high, it would restrict the hybridization between the HP and miRNA-21 because of the steric hindrance effect. Therefore, the optimized concentration of HP was 0.1 μM. The effect of CT concentration on the sensor performance was exhibited in Fig. S1B. As we can see, ΔI increased rapidly with the increasing concentration of CT and plateaued after 0.25 μM CT, suggesting the saturation of the hybridization between the unfolded HP and CT. Thus, 0.25 μM CT was used in the following experiments.

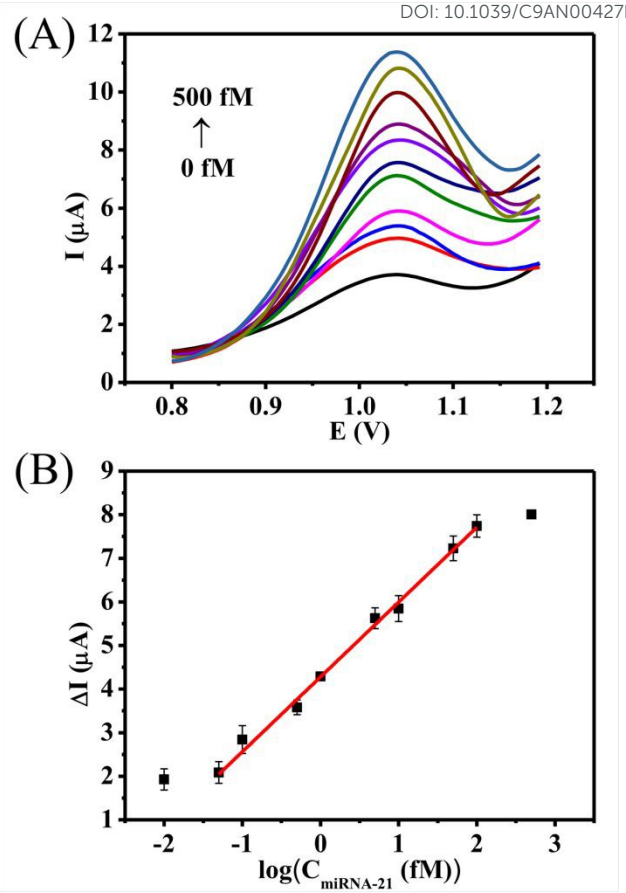

Fig. 5 (A) DPV responses of the developed biosensor towards different concentrations of miRNA-21 (0, 0.01, 0.05, 0.1, 0.5, 1, 5, 10, 50, 100 and 500 fM). (B) The corresponding calibration curve of the miRNA-21 biosensor.

To yield the greatest signal amplification effect, the influence of the RCA reaction time on the sensor performance was investigated and shown in Fig. S1C. At the beginning of the RCA reaction, long DNA product was synthesized and resulted in dramatic increase of ΔI. As the reaction time increased, ΔI kept increasing and reached the highest value at 60 min. Then the reaction reached saturation due to the exhaustion of RCA substrates or the deactivation of phi29 DNA polymerase.[11] Thus, the RCA reaction time of 60 min was selected for the following experiments.

Calibration curve

View Article Online
DOI: 10.1039/C9AN00427K

Table 1 Comparison of the developed biosensor with previous reported electrochemical methods for miRNAs detection.

Targets	Strategies	Linear Range	Detection Limit	Refs
miRNA-141	Enzyme-assisted amplification and dsDNA-templated CuNPs	0.1 fM - 100 fM	45 aM	33
miRNA-199a	Target-assisted polymerization nicking reaction and hybridization chain reaction DNA-templated AgNCs	1 fM - 0.1 nM	0.64 fM	9
miRNA-21	Pt/Sn-In_2O_3 nanoflower with advanced oxygen reduction reaction performance	5 pM - 0.5 fM	1.92 fM	34
miRNA-21	MoS_2 nanosheet functionalized with thionine and gold nanoparticles	1 pM - 10 nM	0.26 pM	35
miRNA-21	Target-triggered Ru(III) release and redox recycling	0.1 fM -1.5 pM	33 aM	36
miRNA-155	3D nitrogen-doped reduced graphene oxide electrode and tetrahedral DNA nanostructure	10 pM - 100 nM	1.0 pM	37
miRNA-142-3p	Self-assembled horseradish peroxidase-based polymer dual signal amplification	1 pM - 10 nM	100 fM	38
miRNA-21	**RCA-mediated PdNPs**	**50 aM - 100 fM**	**8.6 aM**	**This work**

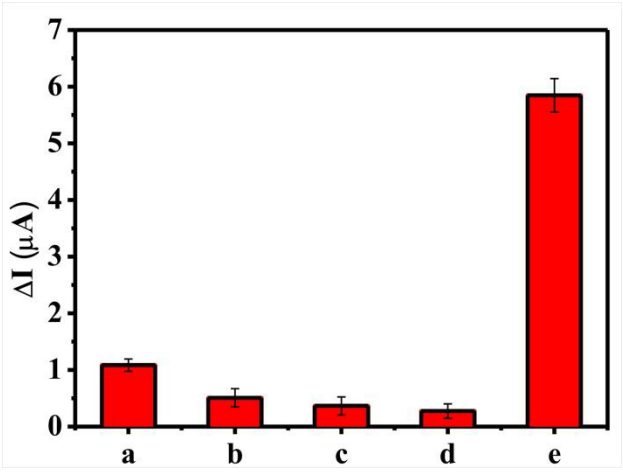

Fig. 6 Reponses of the proposed biosensor towards (a) sRNA, (b) tRNA, (c) miRNA-141, (d) let-7d and (e) miRNA-21 at the same concentration of 10 fM.

Under the optimal experimental conditions, the developed biosensor was employed to detect miRNA-21 with a series of concentrations. As shown in Fig. 5A, ΔI gradually increased with an incremental concentration of miRNA-21 from 0 fM to 500 fM. Moreover, the current variation showed a linear relationship with the logarithm of the miRNA-21 concentration ranging from 50 aM to 100 fM (Fig. 5B). The obtained linear calibration equation was ΔI (μA) = 1.7164 log (CmiRNA-21 (fM)) + 4.2791 with a correlation coefficient of 0.993. The limit of detection was calculated to be 8.6 aM miRNA-21 (based on 3σ rule), which was much lower than the previous reported electrochemical methods for miRNA detection (Table 1). The label-free and ultrasensitive detection of miRNA-21 was achieved by the RCA-mediated PdNPs amplification strategy.

Selectivity, reproducibility and stability

The selectivity of the developed biosensor was evaluated by testing different miRNAs, including miRNA-21, single-base mismatched miRNA-21 (sRNA), three-base mismatched miRNA-21 (tRNA), miRNA-141 and let-7d at the same concentration (10 fM). As illustrated in Fig. 6, the sensor response towards sRNA was fairly slight compared with miRNA-21, while the responses towards tRNA, miRNA-141 and let-7d were almost negligible. The results meant that the developed biosensor exhibited good selectivity for miRNA-21 detection.

To estimate the reproducibility of the developed biosensor, four HP/AuE sensors prepared in the same conditions were used to detect 10 fM miRNA-21. As shown in Fig. S2, the results showed a relative standard deviation (RSD) of 5.2%, indicating acceptable electrode-to-electrode reproducibility of

Table 2 Determination of miRNA-21 in 10-fold diluted healthy human serum (n=3).

Serum samples	MiRNA-21 added (fM)	MiRNA-21 found (fM)	Recovery (%)	RSD (%)
1	0.1	0.11	110	7.33
2	1	0.92	92	2.77
3	10	9.64	96.4	4.58

View Article Online
DOI: 10.1039/C9AN00427K

the developed biosensor.

To investigate the stability of the biosensor, the fabricated HP/AuE sensors were stored at 4 ℃ in a refrigerator for 1, 3, 5, 7 and 15 days, and then used to detect miRNA-21 (Fig. S3). Compared with the freshly fabricated sensor, they exhibited stable responses. Even after 15 days, the sensor was able to maintain 88.1% of the original response, implying that the developed biosensor exhibited favorable stability.

Real Sample Analysis

The applicability of the developed biosensor in complex biological systems has been investigated through spike/recovery experiments, which were performed by spiking different concentrations of miRNA-21 into 10-fold diluted healthy human serum. As presented in Table 2, good recoveries ranging from 92% to 110% were obtained with RSDs less than 7.33%, suggesting that the developed biosensor was a potential tool for determination of miRNA-21 in complex detection systems.

The practical application performance of the proposed biosensor was further demonstrated by detecting miRNA-21 from clinical serum samples extracted from healthy donors and breast cancer patients. These samples were provided by Qilu Hospital of Shandong University and were subsequently diluted 10-fold prior to analysis. As shown in Fig. S4, higher responses were generated for the samples from cancer patients than that from healthy people, indicating up-regulation of miRNA-21 in the serums from breast cancer patients. These results were also consistent with the results reported in literatures,[39,40] demonstrating that the developed biosensor could be a potential tool for clinical detection of miRNA-21.

Conclusions

In summary, an ultrasensitive and label-free electrochemical biosensor for miRNA detection based on RCA-mediated in-situ synthesis of PdNPs was developed. This biosensor exhibited good selectivity and superior sensitivity towards miRNA-21 with an ultralow detection limit of 8.6 aM. These satisfying results were attributed to the following two reasons. One is target-induced RCA which integrated specific target recognition with signal amplification by generating numerous G-rich ssDNAs as signal indicator carrier. Further, the formation of electroactive PdNPs on these G-rich ssDNAs realized the cascade signal amplification. The remarkable sensitivity and selectivity along with the capability for real sample analysis endowed the developed biosensor with a promising potential in early disease diagnosis application. Moreover, the proposed design provides a reference for the combination of molecular biology with nanotechnology for bioanalysis applications.

Conflicts of interest

There are no conflicts to declare.

Acknowledgements

This work was supported by the National Science Foundation of China (21305077), the Natural Science Foundation of Shandong Province (ZR2017BEM020), the Research Award Fund for Outstanding Middle-aged and Young Scientist of Shandong Province (BS2013SW031), the Special Funding of China Postdoctoral Science Foundation (2014T70629), and the Young Scholars Program of Shandong University (2016WLJH04).

Notes and references

1 C. Ye, M. Q. Wang, H. Q. Luo and N. B. Li, *Anal. Chem.*, 2017, **89**, 11697-11702.
2 T. Y. Xue, W. Y. Liang, Y. W. Li, Y. H. Sun, Y. J. Xiang, Y. P. Zhang, Z. G. Dai, Y. H. Duo, L. M. Wu, K. Qi, B. N. Shivananju, L. J. Zhang, X. Q. Cui, H. Zhang and Q. L. Bao, *Nat. Commun.*, 2019, **10**, 28-36.
3 T. Kilic, A. Erdem, M. Ozsoz and S. Carrara, *Biosens. Bioelectron.*, 2018, **99**, 525-546.
4 S. Wang, S. S. Lu, J. H. Zhao, J. Ye, J. S. Huang and X. R. Yang, *Biosens. Bioelectron.*, 2019, **126**, 565-571.
5 K. Mahato, A. Kumar, P. K. Maurya and P. Chandra, *Biosens. Bioelectron.*, 2018, **100**, 411-428.
6 L. Berti and G. A. Burley, *Nature Nanotech.*, 2008, **3**, 81-87.
7 Y. F. Hu, Q. Q. Zhang, Z. Y. Guo, S. Wang, C. N. Du and C. Y. Zhai, *Biosens. Bioelectron.*, 2017, **98**, 91-99.
8 Z. W. Chen, C. Q. Liu, F. F. Cao, J. S. Ren and X. G. Qu, *Chem. Soc. Rev.*, 2018, **47**, 4017-4072.
9 C. Y. Yang, K. Shi, B. T. Dou, Y. Xiang, Y. Q. Chai and R. Yuan, *ACS Appl. Mater. Interfaces*, 2015, **7**, 1188-1193.
10 Y. J. Wang, X. Y. Zhang, L. Zhao, T. Bao, W. Wen, X. H. Zhang and S. F. Wang, *Biosens. Bioelectron.*, 2017, **98**, 386-391.
11 Y. Zhu, H. J. Wang, L. Wang, J. Zhu and W. Jiang, *ACS Appl. Mater. Interfaces*, 2016, **8**, 2573-2581.
12 J. Richter, M. Mertig, W. Pompe, I. Monch and H. K. Schackert, *Appl. Phys. Lett.*, 2001, **78**, 536-538.
13 K. Nguyen, M. Monteverde, A. Filoramo, L. Goux-Capes, S. Lyonnais, P. Jegou, P. Viel, M. Goffman and J. P. Bourgoin, *Adv. Mater.*, 2008, **20**, 1099-1104.
14 W. Li, Y. M. Fu, Y. Fu, X. Wang and J. L. Zhang, *Catal. Lett.*, 2013, **143**, 578-586.
15 J. Richter, *Physica E*, 2003, **16**, 57-173.
16 Y. X. Zhao, F. Chen, Q. Li, L. H. Wang and C. H. Fan, *Chem. Rev.*, 2015, **115**, 12491-12545.
17 C. Russell, S. Roy, S. Ganguly, X. Y. Qian, M. H. Caruthers and M. Nilsson, *Anal. Chem.*, 2015, **87**, 6660-6666.
18 H. X. Ji, F. Yan, J. P. Lei and H. X. Ju, *Anal. Chem.*, 2012, **84**, 7166-7171.
19 F. L. Gao, F. Y. Zhou, S. J. Chen, Y. Yao, J. Wu, D. Y. Yin, D. Q. Geng and P. Wang, *Analyst*, 2017, **142**, 4308-4316.
20 Q. Li, F. P. Zeng, N. Lyu and J. Liang, *Analyst*, 2018, **143**, 2304-2309.
21 B. Q. Liu, B. Zhang, G. N. Chen, H. H. Yang and D. P. Tang, *Anal. Chem.*, 2014, **86**, 7773-7781.
22 Y. N. Guo, Y. Wang, S. Liu, J. H. Yu, H. Z. Wang, Y. L. Wang and J. D. Huang, *Biosens. Bioelectron.*, 2016, **75**, 315-319.
23 T. Kangkamano, A. Numnuam, W. Limbut, P. Kanatharana, T. Vilaivan and P. Thavarungkul, *Biosens. Bioelectron.*, 2018, **102**, 217-225.
24 Y. Li, L. Liang and C. Y. Zhang, *Anal. Chem.*, 2013, **85**, 11174-11179.

25 S. Akhtar, M. Stromberg, T. Z. G. de la Torre, C. Russell, K. Gunnarsson, M. Nilsson, P. Svedlindh, M. Stromme and K. Leifer, *J. Phys. Chem. B*, 2010, **114**, 13255-13262.
26 A. G. Wu, Z. Li, H. L. Zhou and E. K. Wang, *Superlattices Microstruct.*, 2005, **37**, 151-161.
27 M. N. Al-Hinai, R. Hassanien, N. G. Wright, A. B. Horsfall, A. Houlton and B. R. Horrocks, *Faraday Discuss.*, 2013, **164**, 71-91.
28 S. Kundu, K. Wang, D. Huitink and H. Liang, *Langmuir*, 2009, **25**, 10146-10152.
29 Y. Zhu, C. Q. Zhou, X. P. Yan, Y. Yan and Q. Wang, *Anal. Chim. Acta*, 2015, **883**, 81-89.
30 H. Wang and X. B. Ge, *Electroanalysis*, 2012, **24**, 911-916.
31 T. Kilic, A. Erdem, Y. Erac, M. O. Seydibeyoglu, S. Okur and M. Ozsoz, *Electroanalysis*, 2015, **27**, 317-326.
32 Y. L. Geng, J. F. Liu, E. Pound, S. Gyawali, J. N. Harb and A. T. Woolley, *J. Mater. Chem.*, 2011, **21**, 12126-12131.
33 P. Miao, T. Zhang, J. H. Xu and Y. G. Tang, *Anal. Chem.*, 2018, **90**, 11154-11160.
34 K. Zhang, H. F. Dong, W. H. Dai, X. D. Meng, H. T. Lu, T. T. Wu and X. J. Zhang, *Anal. Chem.*, 2017, **89**, 648-655.
35 D. Zhu, W. Liu, D. X. Zhao, Q. Hao, J. Li, J. X. Huang, J. Y. Shi, J. Chao, S. Su and L. H. Wang, *ACS Appl. Mater. Interfaces*, 2017, **9**, 35597-35603.
36 P. P. Gai, C. C. Gu, H. Y. Li, X. Z. Sun and F. Li, *Anal. Chem.*, 2017, **89**, 12293-12298.
37 R. Tian, W. H. Ning, M. H. Chen, C. Zhang, Q. W. Li and J. W. Bai, *Talanta*, 2019, **194**, 273-281.
38 L. L. He, L. H. Ding, S. C. Yu, F. Yu, Y. M. Tian, X. S. Xie, L. B. Qu, L. Liu and Y. J. Wu, *Sens. Actuators B-Chem.*, 2019, **279**, 440-446.
39 C. L. He, M. Q. Wang, X. B. Sun, Y. Zhu, X. Zhou, S. Y. Xiao, Q. J. Zhang, F. N. Liu, Y. Yu, H. J. Liang and G. Zou, *Biosens. Bioelectron.*, 2019, **129**, 50-57.
40 K. Boriachek, M. Umer, M. N. Islam, V. Gopalan, A. K. Lam, N. T. Nguyen and M. J. A. Shiddiky, *Analyst*, 2018, **143**, 1662-1669.

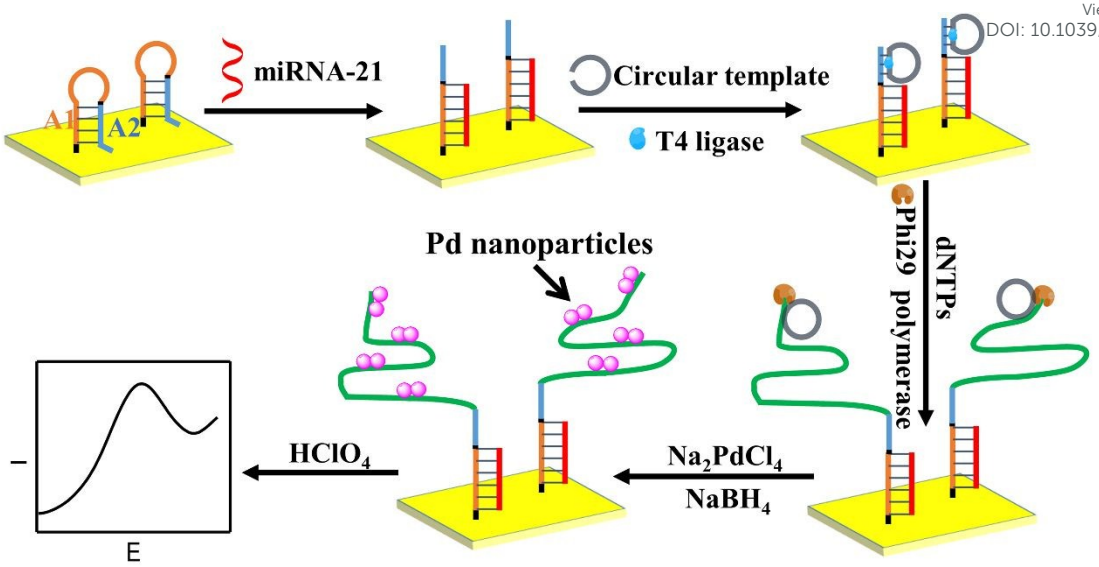

Scheme 1 Schematic illustration of the electrochemical detection of miRNA-21 based on RCA product-mediated synthesis of PdNPs.

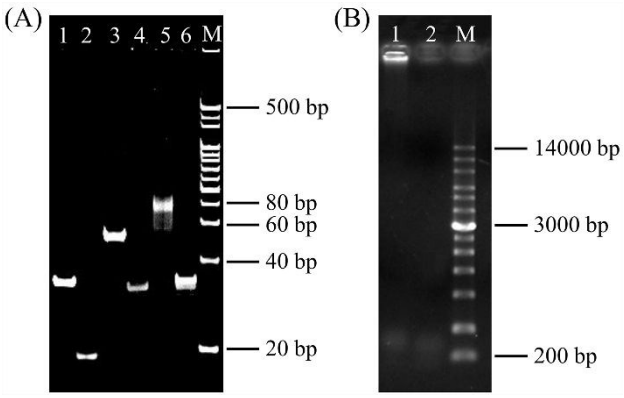

Fig. 1 (A) PAGE images of different samples: (1) HP, (2) miRNA-21, (3) HP + miRNA-21, (4) CT, (5) HP + miRNA-21 + CT + T4 ligase, (6) HP + CT + T4 ligase and (M) marker. (B) Agarose gel electrophoresis analysis: (1) target-induced RCA, (2) control experiment without miRNA-21 and (M) DNA marker.

View Article Online
DOI: 10.1039/C9AN00427K

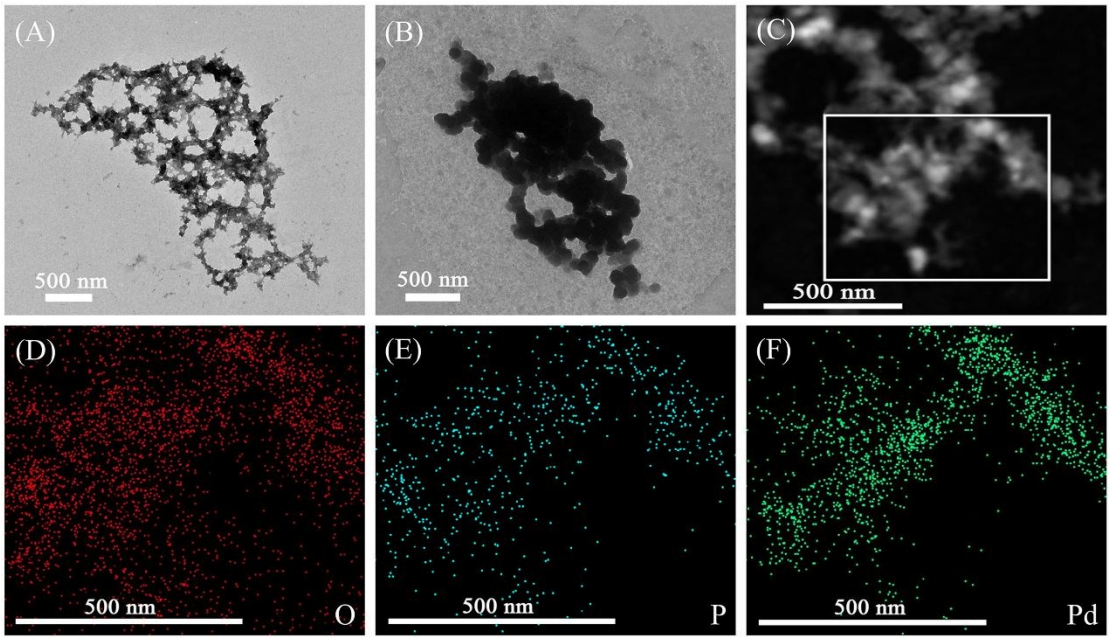

Fig. 2 HRTEM images of (A) RCA product and (B) RCA product-mediated PdNPs. EDS phase distribution images of (C) RCA product-mediated PdNPs for the analysis of (D) O, (E) P and (F) Pd elements.

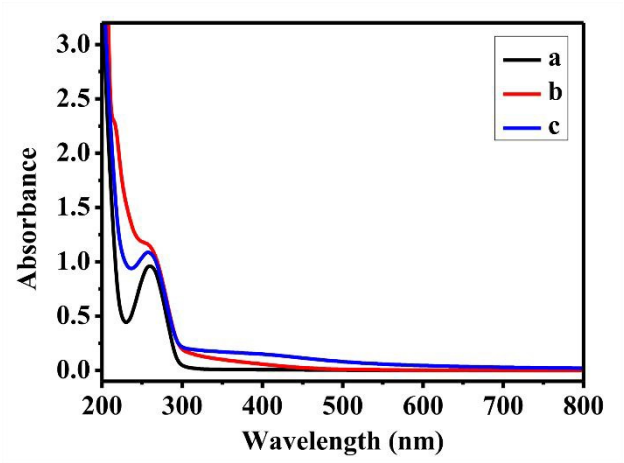

Fig. 3 UV-Vis spectra for (a) G-rich long ssDNA, (b) Na_2PdCl_4/G-rich long ssDNA and (c) PdNPs/G-rich long ssDNA.

View Article Online
DOI: 10.1039/C9AN00427K

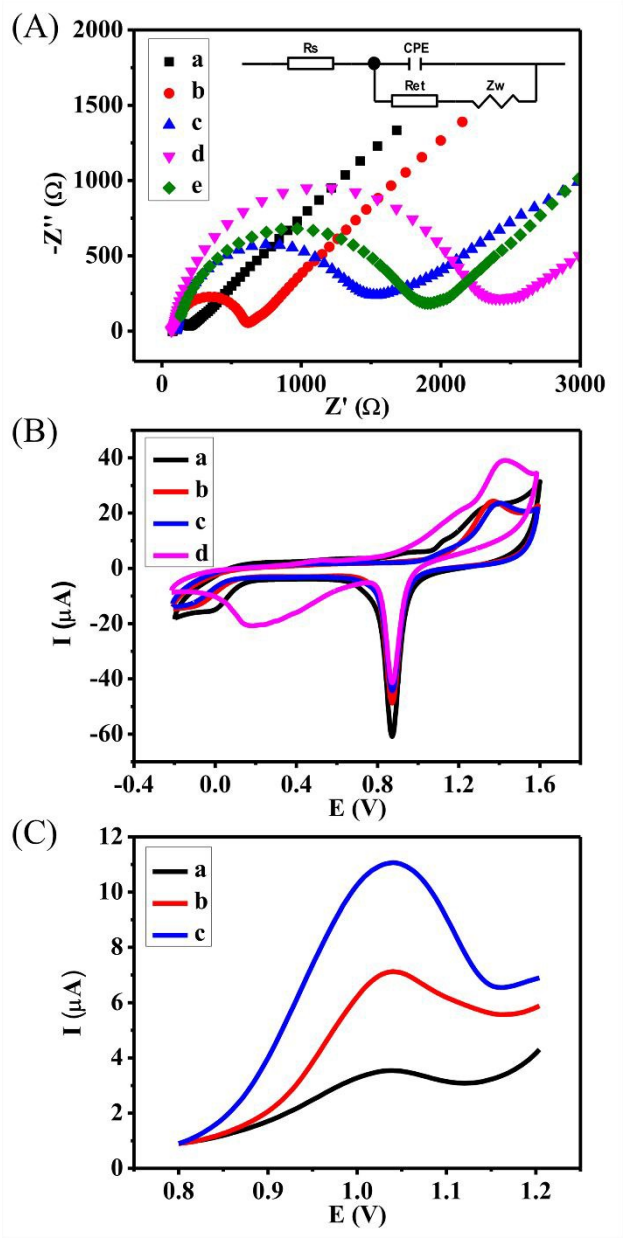

Fig. 4 (A) EIS for (a) bare AuE, (b) HP/AuE, (c) miRNA-21/HP/AuE, (d) RCA product/miRNA-21/HP/AuE and (e) PdNPs/RCA product/miRNA-21/HP/AuE in 0.1 M KCl containing 5.0 mM $[Fe(CN)_6]^{3-/4-}$ in the frequency ranging from 10 mHz to 100 kHz with an amplitude of 5 mV (The inset is the equivalent circuit of the Nyquist plots). (B) CVs for (a) bare AuE, (b) HP/AuE, (c) RCA product/miRNA-21/HP/AuE and (d) PdNPs/RCA product/miRNA-21/HP/AuE in 0.1 M $HClO_4$ by scanning the potential from -0.2 to 1.6 V with a scan rate of 50 mV/s. (C) DPVs of the biosensor in different concentrations of miRNA-21: (a) 0 fM, (b) 1 fM and (c) 100 fM.

View Article Online
DOI: 10.1039/C9AN00427K

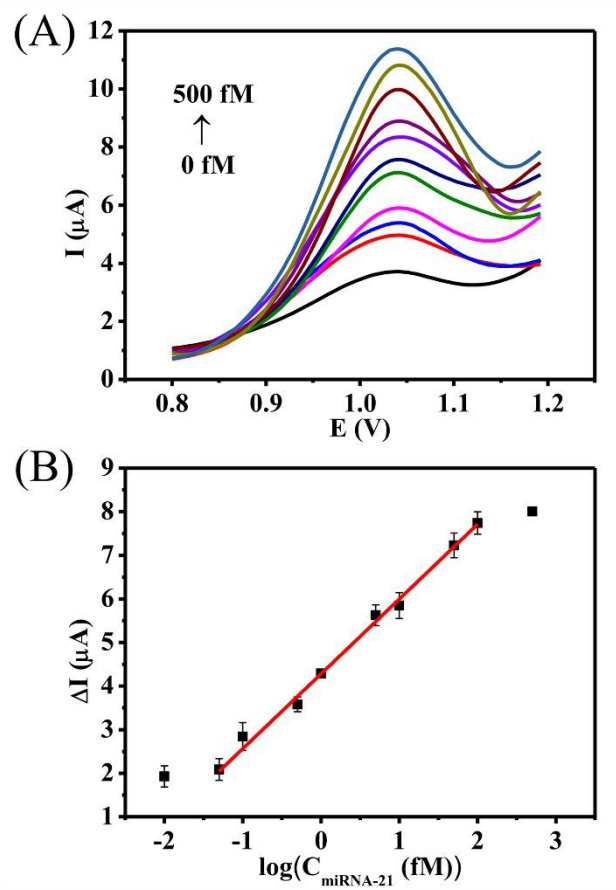

Fig. 5 (A) DPV responses of the developed biosensor towards different concentrations of miRNA-21 (0, 0.01, 0.05, 0.1, 0.5, 1, 5, 10, 50, 100 and 500 fM). (B) The corresponding calibration curve of the miRNA-21 biosensor.

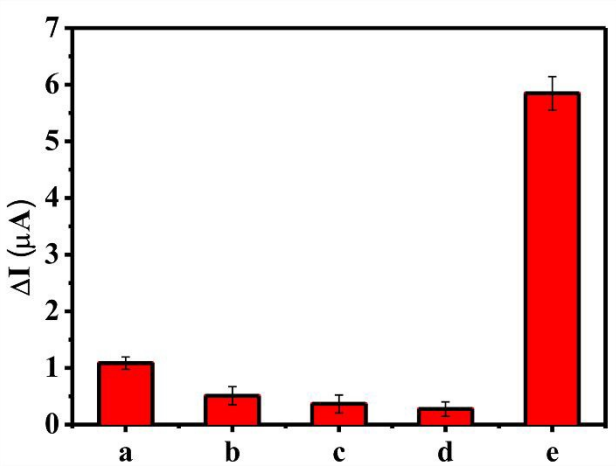

Fig. 6 Reponses of the proposed biosensor towards (a) sRNA, (b) tRNA, (c) miRNA-141, (d) let-7d and (e) miRNA-21 at the same concentration of 10 fM.

View Article Online
DOI: 10.1039/C9AN00427K

An ultrasensitive and label-free electrochemical biosensor for microRNA was developed based on rolling circle amplification-mediated palladium nanoparticles.

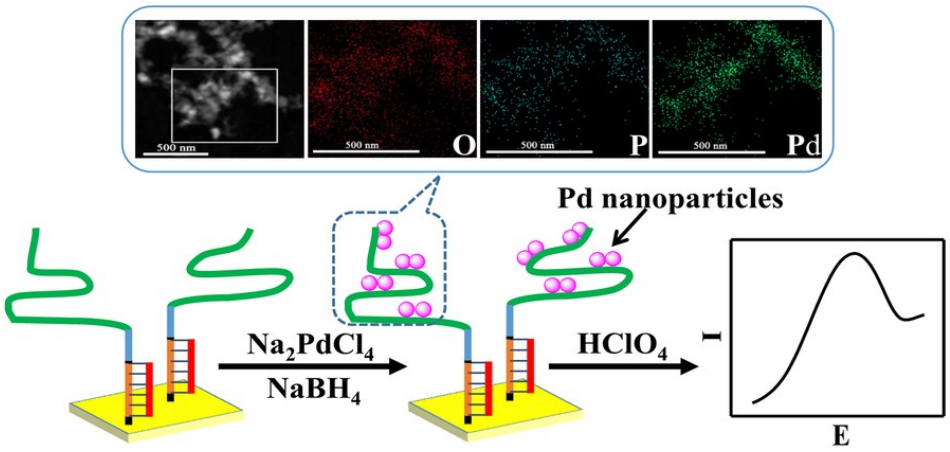

80x40mm (300 x 300 DPI)